JOURNAL OF MATERIALS SCIENCE **34** (1999) 1721–1728

Microstructure of X52 and X65 pipeline steels

J. Q. WANG*, A. ATRENS, D. R. COUSENS, N. KINAEV
Department of Mining, Minerals and Materials Engineering, The University of Queensland, Brisbane, QLD Australia 4072
E-mail: atrens@minmet.uq.oz.au

The microstructure of two commercial pipeline steels X52 and X65 was examined to provide a foundation for the understanding of the IGSCC mechanism of pipeline steels. Observation of the microstructure was carried out using scanning electron microscopy (SEM) and an analytical electron microscope. The microstructure of X52 and X65 pipeline steels shows banding of pearlite rich and ferrite rich areas. The ferrite grains were about 10 μm in size with curved grain boundaries. There was carbide at the ferrite grain boundaries for X52 steel, and there was circumstantial evidence to suggest carbon segregation at the boundaries. The pearlite colonies were consistent with nucleation by a number of different mechanisms.

1. Introduction

Understanding the microstructure of pipeline steels is an important aspect required for the understanding of the mechanism of intergranular stress corrosion cracking (IGSCC), which is a significant failure mode for pipelines [1–6]. Henthorne and Parkins [7] observed that corrosion occurs along grain boundaries (gbs) in the absence of stress, and that anodic polarization can cause virtual disintegration of unstressed carbon steel by intergranular corrosion. This implies that carbon steels contain paths susceptible to corrosion, and that their distribution is related to the paths followed by stress corrosion cracking (SCC). Parkins [3] proposed that the IGSCC mechanism involves the interaction of the (applied) stress and corrosion of the preexisting paths. Furthermore, the work of Henthone and Parkins [7] indicated that the corrosion is related to the presence of carbon or carbides at the ferrite gbs.

Steelmaking for pipelines is an involved and complex process, therefore, there may be different microstructures for different pipeline grades. The temperature and holding times influence the ferrite carbon solubility and carbon segregation to gbs [8]. Carbides can precipitate at the ferrite gbs during the austenite transformation, and this process is strongly related to the cooling rate and Mn content [9, 10].

Our previous work [11–13] used analytical electron microscopy to measure grain boundary (gb) composition of X52 and X65 pipeline steel. All elements of interest were examined, with the exception of carbon. With this caveat, there was no segregation at proeutectoid ferrite gbs. This lack of segregation indicated that the commonly expected species S and P were not responsible for preferential corrosion of gbs during intergranular stress corrosion cracking of pipeline steels. Mn was the only species measured to segregate at the other boundaries. Mn segregated to the boundaries between pro-eutectoid ferrite and pearlitic cementite, and desegregated from the boundaries between proeutectoid ferrite and pearlitic ferrite. The pearlitic cementite was Mn rich. There was no Mn segregation at the boundaries between pearlitic ferrite and pearlitic cementite. The pattern of Mn segregation could be explained in terms of diffusion in the process zone ahead of the pearlite during the austenite to pearlite transformation and diffusion in the boundaries between the proeutectoid ferrite and pearlite.

The present study of the microstructure of pipeline steels has been carried out to provide a foundation for the understanding of the IGSCC mechanism of pipeline steels. Detailed observation of the microstructure of pipeline steels X52 and X65 was carried out using scanning electron microscopy (SEM) and an analytical electron microscope. This is part of ongoing research in the area of environmental fracture [24–33].

2. Experimental

The materials studied were X52 and X65 pipeline steels from production pipelines. Such steels are hot rolled at elevated temperatures when they have an austenite (γ) crystal structure followed by relatively rapid cooling [34, 35]. During the rapid cooling the γ partially transforms to proeutectoid ferrite, α, and the remaining γ transforms to pearlite, which leads to their microstructure of proeutectoid α plus pearlite as illustrated in Figs 1 and 2. The pearlite consists of pearlitic ferrite (designated as α_P, to distinguish it from proeutectoid ferrite) and cementite, C_P. The chemical composition (in wt %) is listed in Table I.

* Also affiliated with State Key Laboratory of Corrosion Science, Institute of Corrosion and Protection of Metals, Chinese Academy of Sciences, Shenyang 110015, P. R. China.

TABLE I Steel chemical compositions (in wt %)

Steel	C	Mn	Si	S	P	Ni	Cr	Nb	Al
X52	0.16	1.32	0.31	0.006	0.017	0.01	0.01	0.02	0.03
X65	0.07	1.36	0.19	0.002	0.013	0.01	0.2	0.04	0.011

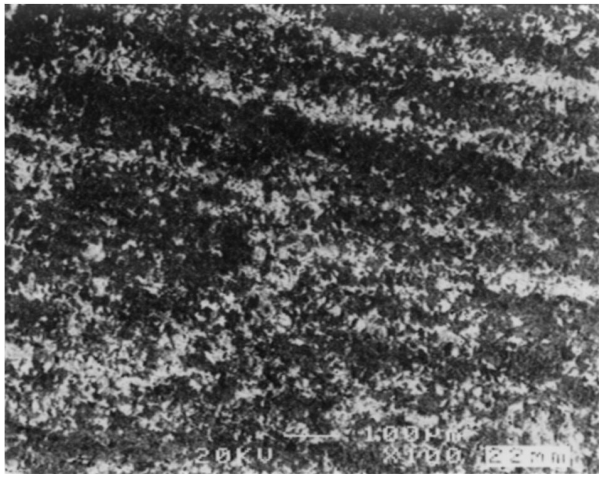

(a)

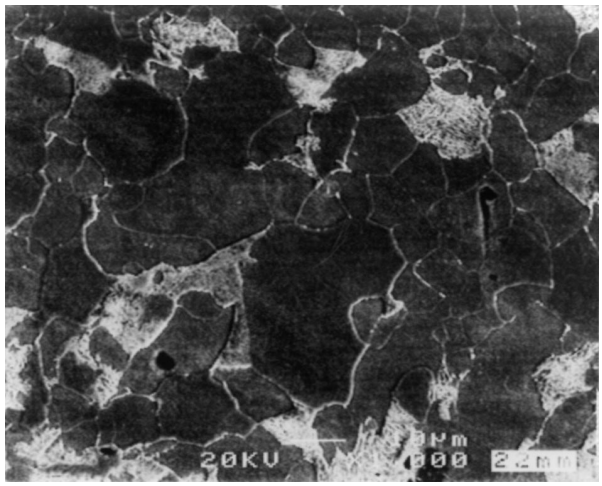

(b)

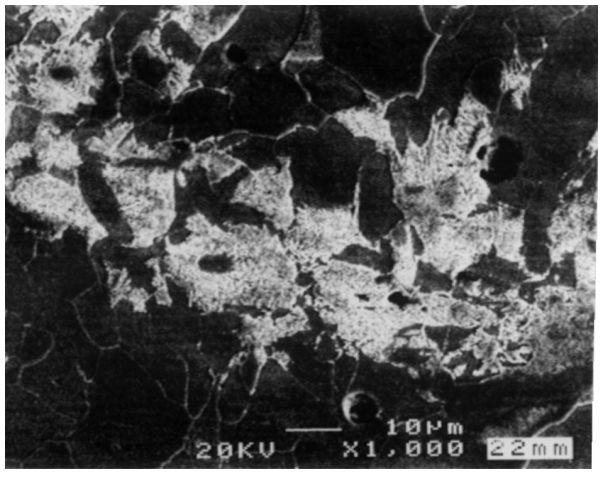

(c)

Figure 1 Microstructure of X52 consisted of ferrite and pearlite (a) banded structure; (b) isolated pearlitic colonies; and (c) interconnected pearlitic colonies.

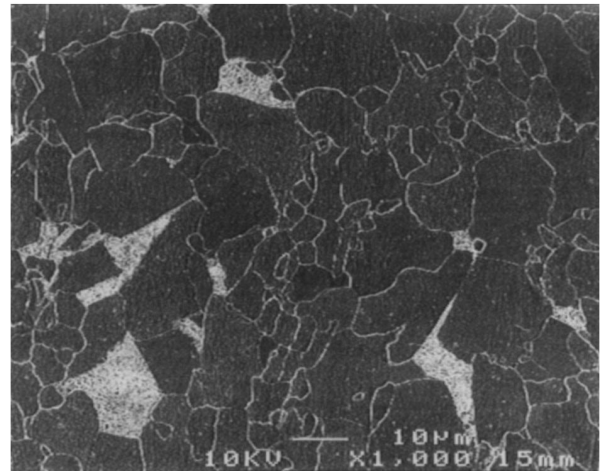

(a)

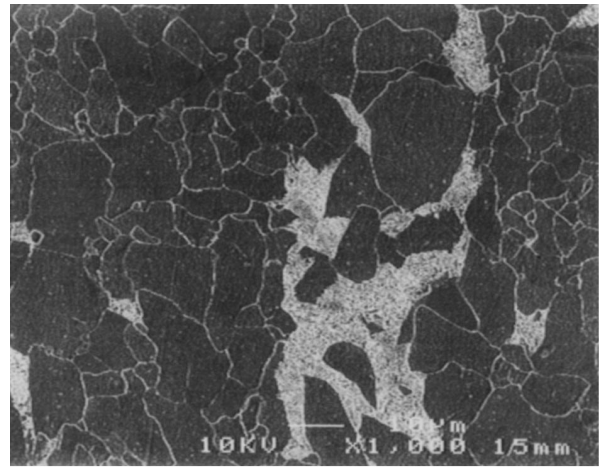

(a)

Figure 2 Microstructure of X65 consisted of ferrite and pearlite (a) isolated pearlitic colonies; (b) interconnected pearlitic colonies.

Pieces of steels were cut from a section of pipe taken from service pipelines, polished from 240 to 1200 grit silicon paper and 6 μm and 1 μm diamond paste, lightly etched using nital, and characterized using the JEOL 6400 SEM. Samples were also deeply etched in nital for 2 min, platinum coated, and then characterized using SEM. Deep etching removed both α and α_p leaving the C_p revealing details of the carbides.

Thin ($\sim$2 μm) cross-section TEM samples were prepared [11–13] in order to have acceptable EDS signal to noise values from gbs segregation and to minimize the amount of ferromagnetic steel in the analytical electron microscope, VG HB601. These samples were thinned using ion milling.

3. Results and discussion

3.1. Overview of the microstructure

The microstructure of X52 and X65 after light etching is shown in Figs 1 and 2. The microstructure consisted of proeutectoid α and pearlite. The microstructure at low magnification showed banding with ferrite rich and pearlite rich areas elongated along the rolling direction as shown in Fig. 1a. The proeutectoid ferrite fractions are consistent with calculations based on the carbon

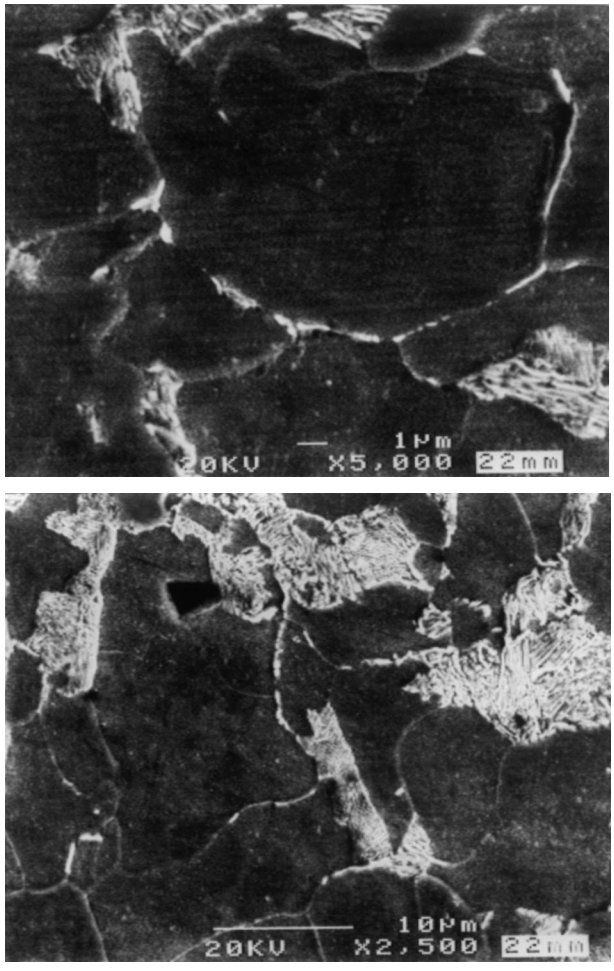

Figure 3 Grain boundary carbides at α/α gbs for X52 steel.

content, which give 0.93 for X65 containing 0.07% C and 0.79 for X52 containing 0.16% C. The lower carbon content for X65 leads a pearlite fraction lower than that of X52. The pearlite colonies for both steels were most likely isolated in the ferrite rich bands as shown in Figs 1b and 2a, whereas the pearlite was interconnected in the pearlite rich bands as shown in Figs 1c and 2b. The size of the isolated pearlite was small compared to the interconnected pearlite. The isolated pearlite colonies mostly occurred at triple points or at α/α grain boundaries.

3.2. α-phase

The α grain shape was irregular as shown in Fig. 1 for X52 and Fig. 2 for X65. The grain size was about 10 μm. Most of gbs were curved as shown in Figs 3 and 4. IGSCC for pipeline steels is more likely to be along the α/α gbs because these are the only continuous paths through the microstructure. Detailed SEM observation of the α/α gbs showed carbide at this kind of grain boundary for X52 as shown in Fig. 3. The gb carbides were not continuous. No clear evidence for gb carbides was observed at α/α gbs for X65, although there were fine carbides inside the α grains for X65 as shown in Fig. 4.

During the γ to α transformation, carbon is rejected from the γ, which has a carbon concentration equal to the bulk steel composition. If the carbon diffusion is not sufficiently fast, carbon will accumulate at the interface

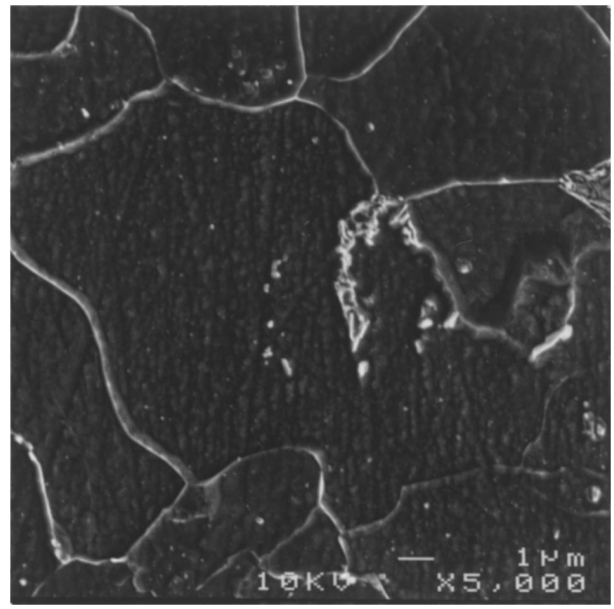

Figure 4 Curve ferrite grain boundaries and carbide inside ferrite grain.

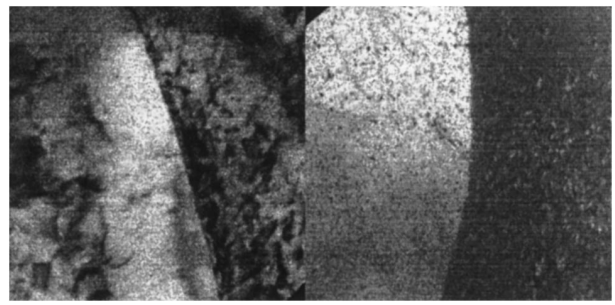

(a) X52 (b) X65

Figure 5 α/α gbs observed using AEM.

of α and γ, and carbide will precipitate at the interface when the carbon content reaches a critical value [36]. Such gb carbides between α grains were observed by Mintz [9] for hypo-eutectoid steels. Mintz found that thinner gb carbides were associated with higher cooling rates and higher Mn contents. The higher cooling rate decreased the amount of carbon available by decreasing the time available for carbon diffusion. The higher Mn contents also limited the amount of carbon available to form gb carbides by slowing down the rate of carbon diffusion. Our observations are consistent with these trends. There were gb carbides for X52 with the higher carbon content and no observed gb carbides for X65 with the lower carbon content.

AEM observation of the α/α gbs, Fig. 5, indicted clean gbs for both steels. No carbides were observed at the gbs, and there were no carbides inside the α grains. The AEM specimens reflect a small volume of material, and consequently, it is not surprising that the AEM specimen did not contain a large gb carbide of the size of those in Fig. 4.

Mn compositional profiles across α/α gbs are shown in Fig. 6. Carbon segregation is expected, but the carbon concentration could not be measured because of the ubiquitous carbon contamination on the sample surface, which is inevitably picked up during sample preparation

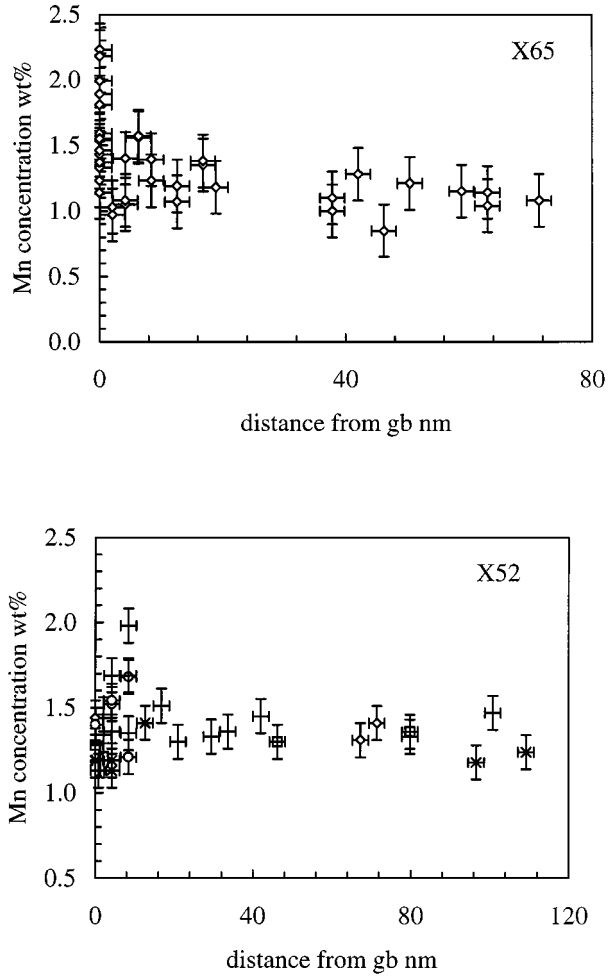

Figure 6 Measured Mn profile across α/α gbs for X65 and X52, respectively.

and transport. There was no trace of other gb embrittlers such as P and S. The measured Mn profile, Fig. 6a, for X65 showed some Mn segregation at this gb, but there was only a hint of segregation for X52, Fig. 6b. Mn was thought to be another rate controlling factor during the γ to α transformation [37]. However, the compositional measurements for X65 and X52 [11–13] showed that the average Mn content in pearlite was similar to that in α. There was no significant difference of Mn content between the α grains and the pearlite colonies. The Mn distribution was more likely to be related to the carbon distribution. The mechanism for Mn to slow down C diffusion is for C atoms to drag along Mn atoms. Therefore a tendency for Mn gb segregation as observed for X65, even though this tendency was slight, would be expected to indicate segregation of C. Thus, our observations are consistent with the expectations of Parkins [3, 7] that IGSCC for pipeline steel results from C segregation at the α/α gbs.

3.3. Pearlite

After the γ to α transformation, the remaining γ transforms to pearlite. Pearlite formation is an age-old topic. The traditional mechanism of pearlite formation is edgeways growth and sideways nucleation [38–40] as illustrated in Fig. 7a. More recent observations showed that pearlite could nucleate at grain triple points [37] as

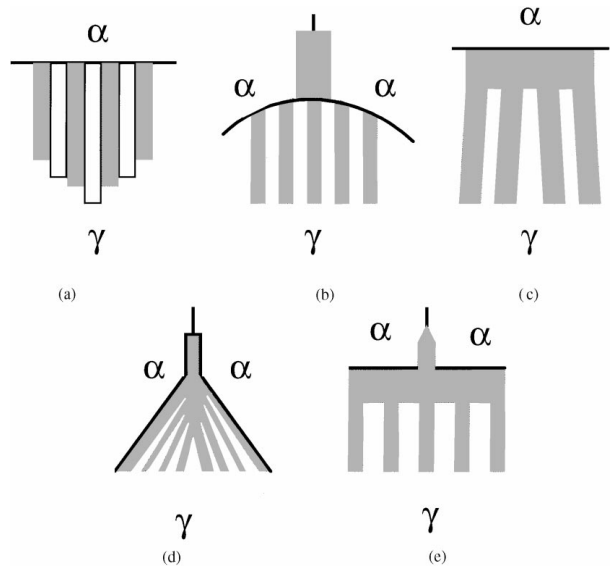

Figure 7 Mechanisms of pearlite formation (a) traditional mechanism of nucleation at α/γ IB; (b) mechanism of pearlite formation from carbide at $\alpha:\alpha$ GB; (c) mechanism of pearlite formation from carbide that first forms at $\alpha:\gamma$ interface; (d) mechanism of pearlite formation by growth and branching from a carbide at the $\alpha:\alpha$ GB; (e) mechanism of pearlite formation from grain boundary carbide.

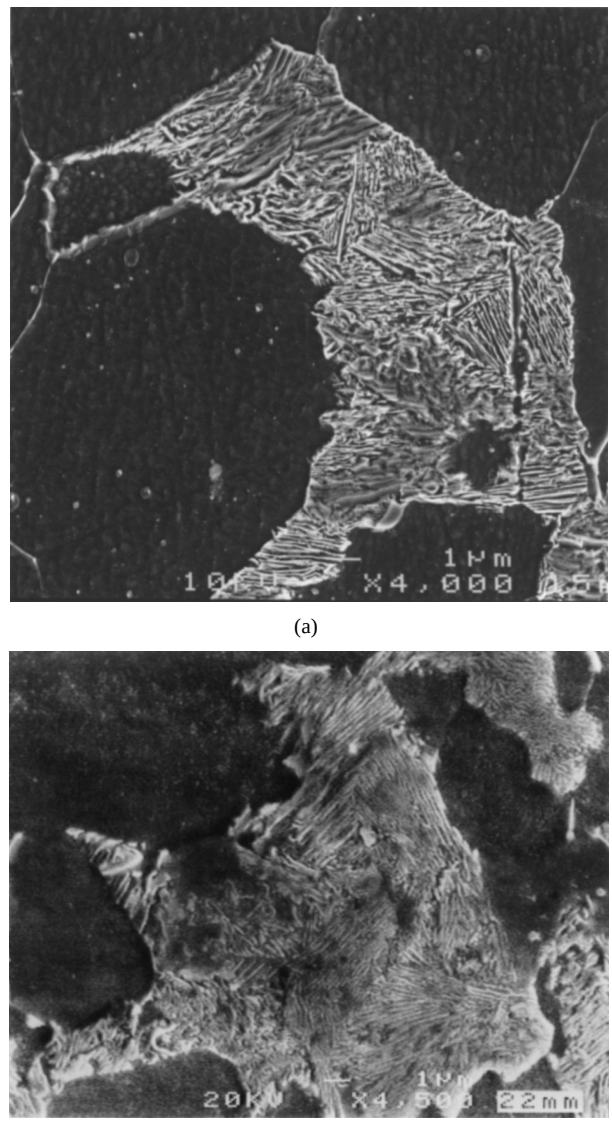

(a)

(b)

Figure 8 Multiple pearlite nucleation. (a) X65 (b) X52.

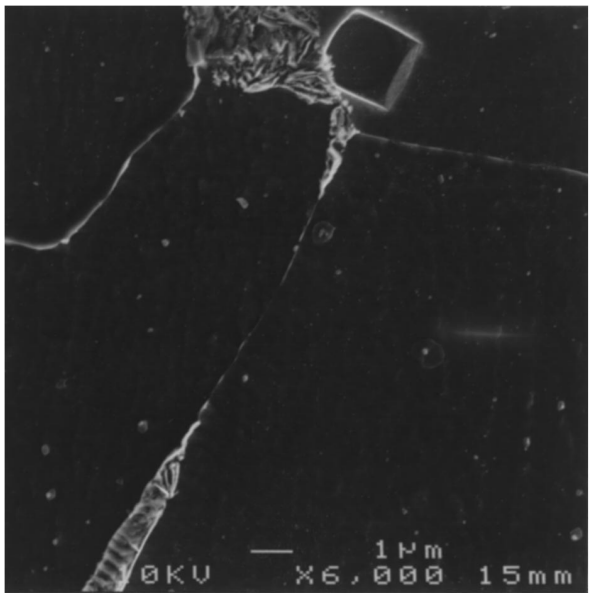

(a)

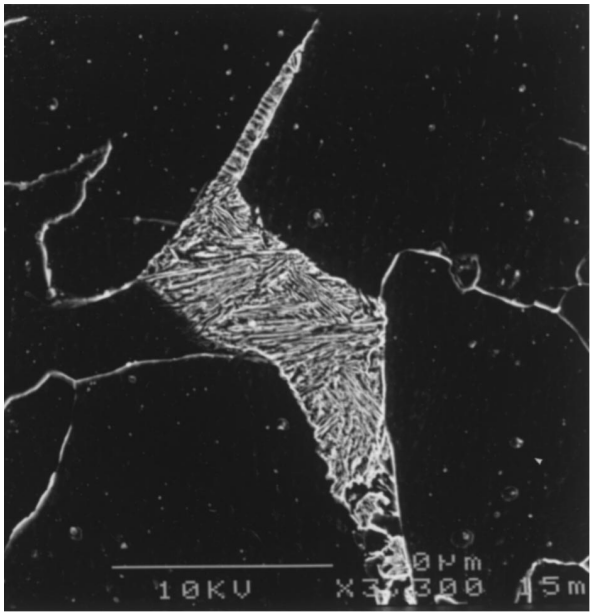

(b)

(c)

Figure 9 Detailed observations of pearlite at both end of ferrite gb for X65 (a) pearlite growth at both ends of a ferrite gb; (b) narrow pearlite colony; and (c) the tip of pearlite colony.

illustrated in Fig. 7b. Zhang and Kelly [36, 41] proposed that rejection of carbon from the transforming austenite in hypoeutectoid steels can lead to the formation of an interface carbide that can nucleate pearlite as illustrated in Fig. 7c. Wang *et al.* [13] suggested the hybrid mechanisms illustrated in Fig. 7d and 7e. After nucleation, pearlite growth often involves branching [36, 41].

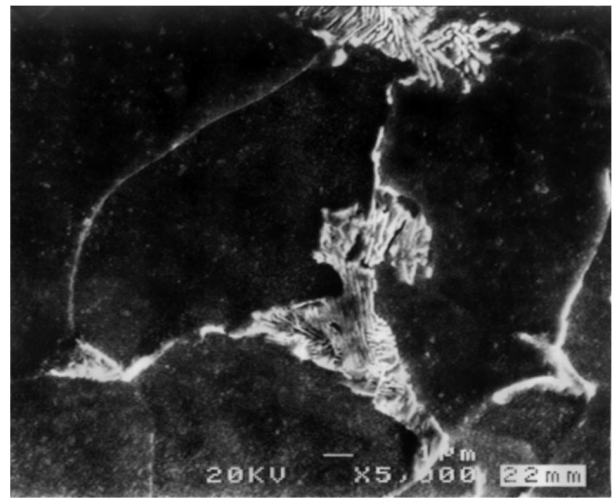

Figure 10 Detailed observation of pearlite at both ends of a ferrite gb for X52.

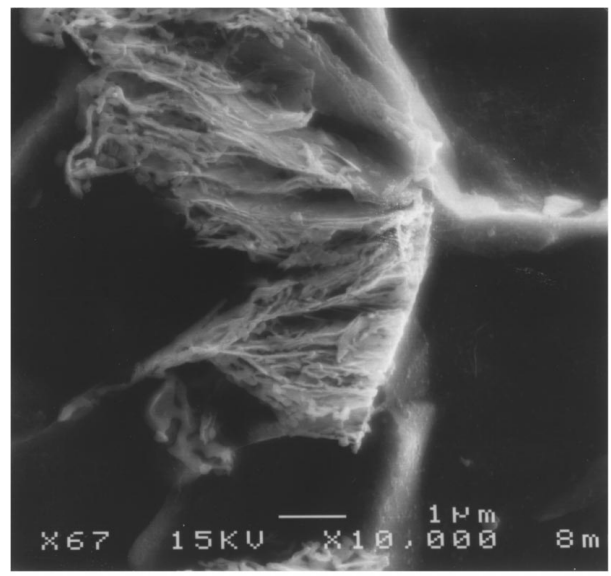

(a) micrograph

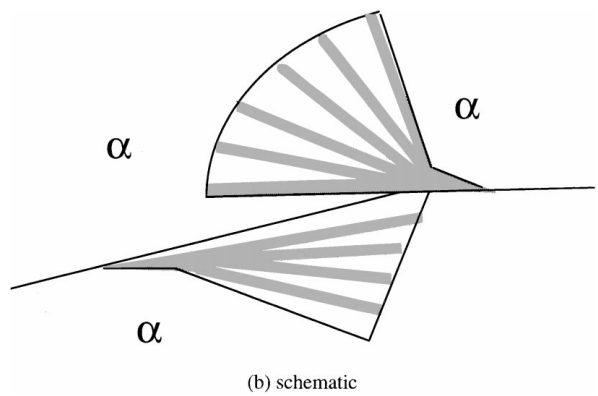

(b) schematic

Figure 11 Pearlite nucleation from grain boundary carbides for X65; (a) micrograph; (b) schematic illustration.

Fig. 8 shows that a typical pearlite colony has multiple nuclei, with Fig. 8a presenting some examples similar to the mechanism illustrated in Fig. 7d. Several pearlite packets impinged on each other, and the pearlite packets have different orientations. For X52, the number of pearlite colonies was greater than that for X65. Narrow pearlite at the triple point of α and pearlite for both steels are shown in Figs 9c and 10 for X65 and X52, respectively. The tips of the narrow pearlite are carbide plates suggesting pearlite nucleation by the mechanism of Fig. 7d. At the other end of the same gb, there was also fine pearlite with carbide tips as shown in Figs 9a and 10. Fine carbide tips of pearlite at both ends of this α/α gb suggest carbon segregation at these gbs.

Fig. 11a shows two gb carbides (GBC_f) that have formed at the triple points, and have nucleated pearlite as illustrated schematically in Fig. 11b. Fig. 12 shows a similar case for X52, the gb carbide, GBC_f at the triple point has nucleated pearlite, which has grown by

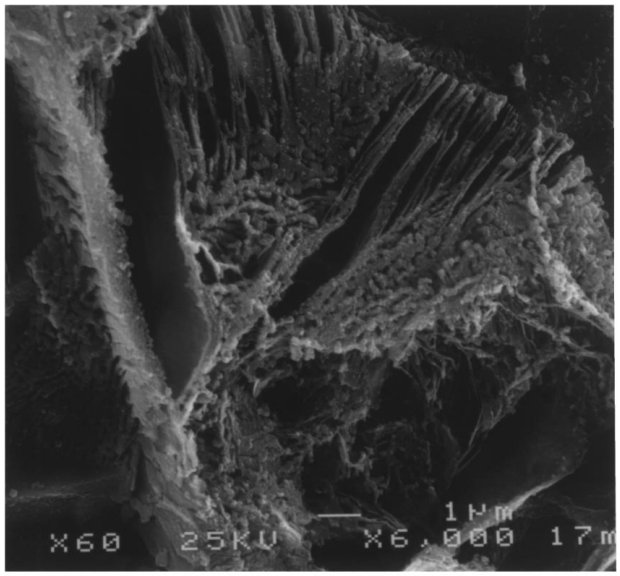

(a) micrograph

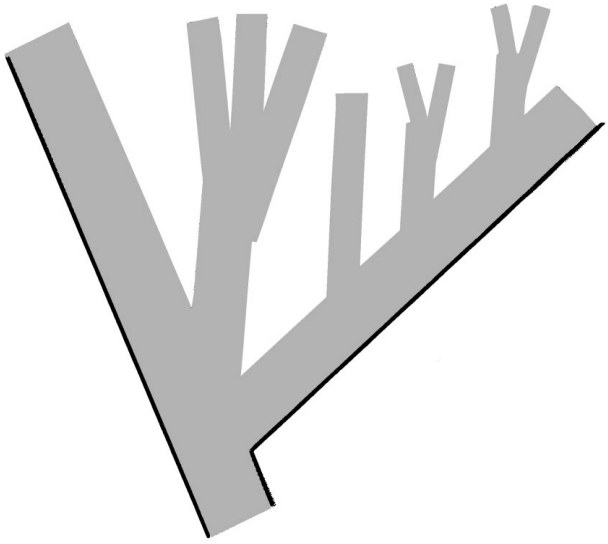

(b) schematic

Figure 12 Grain boundary carbide at the triple point for X52 (a) micrograph; (b) schematic.

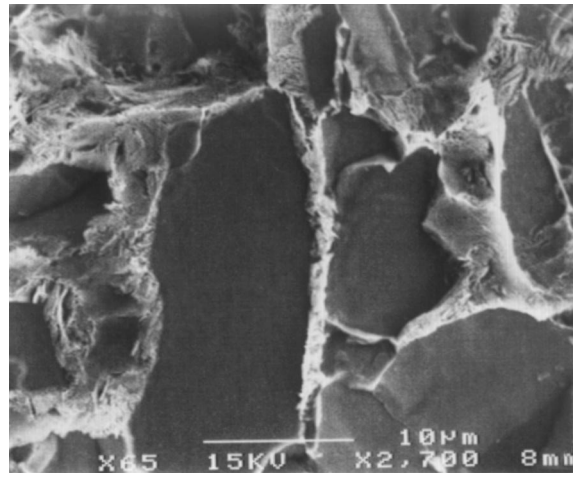

(a)

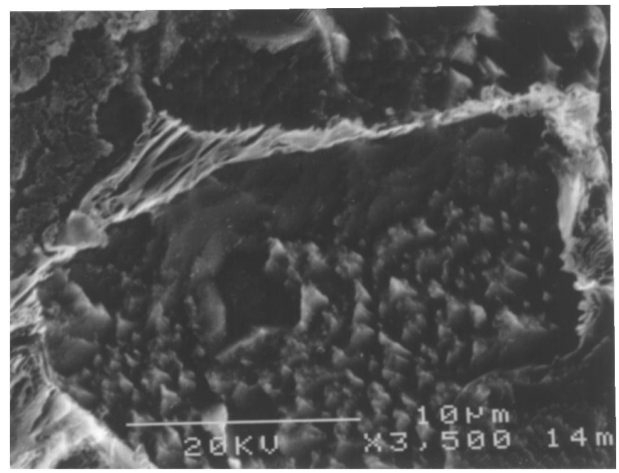

(b)

Figure 13 Narrow pearlite between ferrite grains (a) X65; (b) X52.

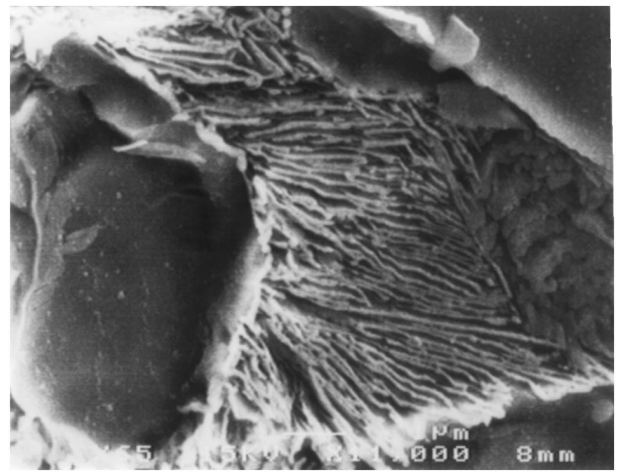

Figure 14 Pearlite nucleation from a gb carbide for X65.

branching. These are further examples of the pearlite nucleation mechanism illustrated in Fig. 7(d).

Several very fine pearlite colonies between two α grains are shown in Fig. 13. The size of fine pearlite is about 1$\sim$2 μm.

A pearlite colony, perpendicular to the surface, is shown in Fig. 14 for X65. The adjacent α grain has been etched away. The pearlite nucleated from a carbide at the α/pearlite boundary, by the mechanism shown in

Fig. 7c. Further examples are shown in Figs 15 and 16. The pearlite grew by branching. The gb carbide in Figs 15 and 16 was a cuboid that nucleated pearlitic carbide, C_p. The C_p was narrower than the gb carbide.

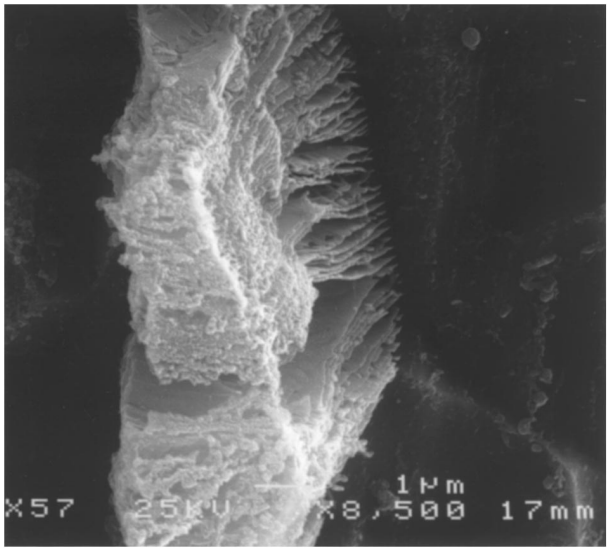

Figure 15 Pearlite growth from a gb carbide for X52.

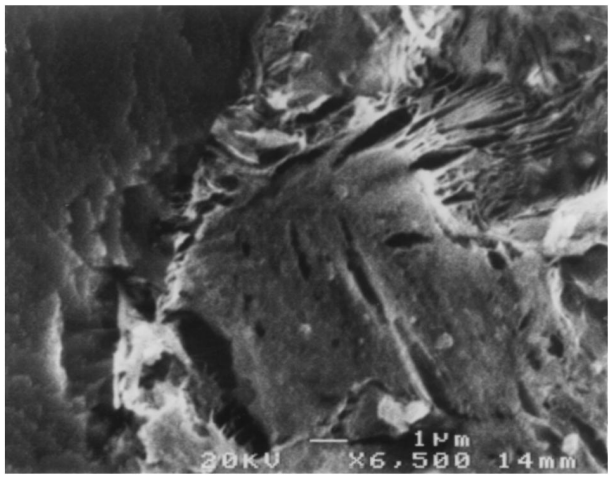

Figure 16 Pearlite growth from a gb carbide for X52.

There was obvious C_p branching in this case, and the spacing between C_p lamellae changed from one layer to the next. Fig. 16 shows a carbide plate at the α/pearlite interface that has nucleated pearlite for X52, and the pearlite has grown by branching. This pearlite mechanism, illustrated in Fig. 7c, is that carbon accumulated at the interface between α and γ during the γ-α transformation, when the carbon content reached a critical value, carbide nucleated at the interface, and the pearlite nucleated from the boundary carbide.

Fig. 17 shows examples of AEM observations of the α/pearlite grain boundary for X65 and X52 steels. The pearlitic carbide often have enlarged areas at the gb and usually have big heads as illustrated in Fig. 17b.

Fig. 18 shows an extremely interesting case, which suggested the new mechanism of pearlite nucleation as illustrated in Fig. 7e. There was a gb carbide (GBC_f) between two α grains. The carbide GBC_f widened gradually from a small nucleus. This gb carbide was very

Figure 18 Grain boundary carbides at the triple junction and α/pearlite grain boundary.

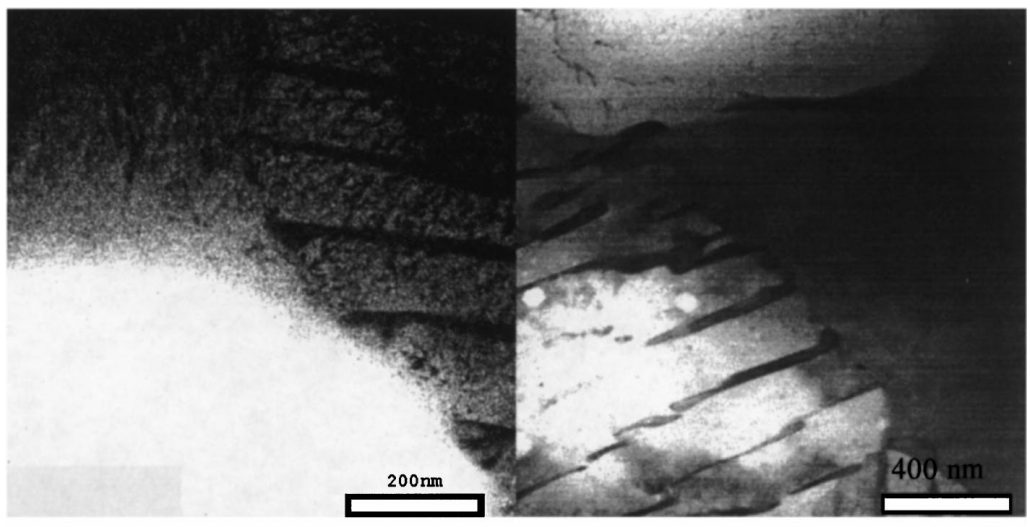

(a) X52 (b) X65

Figure 17 α/pearlite gbs for X52 and X65 steels by STEM.

close to a carbide (IBC_{fp}) at the interface between proeutectoid ferrite and pearlite. Furthermore, pearlite radiated out from the carbide IBC_{fp}. The new model is illustrated in Fig. 7e. A carbide GBC_f precipitates at the α/α GB during the transformation from γ to α, (i.e. during the formation of proeutectoid ferrite from the austenite). During this process, carbon is rejected from the ferrite, and accumulates at the α/γ interface. When this carbon concentration reaches a critical value, carbide precipitates at the α/γ interface (Fig. 7c) as suggested by Zhang and Kelly. Furthermore, Fig. 7e suggested that the carbide at the α/γ interface is nucleated by the carbide GBC_f at the α:α GB. Subsequently, the carbide IBC_{fp}, nucleates the pearlite as in the model of Zhang and Kelly.

4. Conclusions

The microstructure of X52 and X65 pipeline steels shows banding of pearlite rich and ferrite rich areas. The grains were about 10 μm in size with curved grain boundaries. There was carbide at the ferrite grain boundaries for X52 steel, and circumstantial evidence to suggest carbon segregation at the boundaries. The pearlite colonies were consistent with nucleation by a number of different mechanisms.

Acknowledgement

The authors are grateful for the support of East Australian Pipeline Limited, and for a University of Queensland External Support Enabling Grant. The authors would also like to thank EMU, University of Sydney and the CMM staff at the University of Queensland.

References

1. "Final staff report on investigation of Tennessee Gas Transmission Company Pipeline No. 100-1 failure near Natchitoches, Louisiana, March 1965" (Federal Power Commission, Bureau of Natural Gas, Washington D.C., 1965).
2. P. J. KENTISH, *Br. Corros. J.*, **20** (1985) 139.
3. R. N. PARKINS, 5th Symposium on line pipe research, American Gas Association Inc, 1974, paper V, U1–40.
4. R. N. PARKINS, E. BELHIMER and W. K. BLANCHARD Jr, *Corrosion*, **49** (1993) 951.
5. J. A. BEAVERS, T. K. CHRISTMAN and R. N. PARKINS, "Materials Performance," 1998, p. 22.
6. Z. F. WANG and A. ATRENS, Metall. and Mater. Trans. **27A** (1996) 2686.
7. M. HENTHORNE and R. N. PARKINS, *Br. Corros. J.* **7** (1967) 186.
8. P. M. ROBINSON and P. N. RICHARDS *J. Iron Steel Inst.* (1965) 621.
9. B. MINTZ and P. CAMPBELL, *Mater. Sci. Tech.* **5** (1989) 155.
10. B. MINTZ, S. TAJIK and R. VIPOND, *ibid.* **10** (1994) 89.
11. J. Q. WANG, A. ATRENS, D. R. COUSENS, P. M. KELLY, C. NOCKOLDS and A. ATRENS, *Acta Materialia*. **46** (1998) 5677.
12. J. Q. WANG, D. R. COUSENS, C. NOCKOLDS and A. ATRENS, Corrosion & Prevention 97, 1997.
13. J. Q. WANG, A. ATRENS, D. R. COUSENS, C. NOCKOLDS and S. BULCOCK, *J. Mater. Sci.* **33** (1998) 1.
14. A. ATRENS and Z. F. WANG, *ibid.* **33** (1998) 405.
15. A. ATRENS and A. OEHLERT, *ibid.* **33** (1998) 783.
16. A. OEHLERT and A. ATRENS, *ibid.* **33** (1998) 775.
17. *Idem, ibid.* **32** (1997) 6519.
18. A. ATRENS, Z. F. WANG and J. Q. WANG, *Advances in Fracture Research*, in Proceedings of the Ninth International Conference on Fracture, edited by B. L. Karihaloo et al. (Pergamon, 1997) p. 375.
19. A. OEHLERT and A. ATRENS, *Corrosion Sci.* **38** (1996) 1159.
20. *Idem. Act Metallurgica et Materialia* **42** (1994) 1493.
21. A. ATRENS and Z. F. WANG, *Materials Forum* **19** (1995) 9.
22. A. ATRENS, C. C. BROSNAN, S. RAMAMURTHY, A. OEHLERT and I. O. SMITH, *Measurement Science and Technology* **4** (1993) 1281.
23. S. RAMAMURTHY and A. ATRENS, *Corrosion Science* **34** (1993) 1385.
24. A. ATRENS, R. COADE, J. ALLISON, H. KOHL, G. HOCHORTLER and G. KRIST, *Materials Forum* **17** (1993) 263.
25. A. S. LIM and A. ATRENS, *Applied Physics A.* **54** (1992) 270.
26. S. JIN and A. ATRENS, *ibid.* **50** (1990) 287.
27. *Idem. ibid.* **42** (1987) 149.
28. R. M. RIECK, A. ATRENS and I. O. SMITH, *Met. Trans.* **20A** (1989) 889.
29. A. ATRENS, W. HOFFELNER, T. W. DUERIG and J. ALLISON, *Scripta, Met.* **17** (1983) 601.
30. A. ATRENS, *Corrosion* **39** (1983) 483.
31. J. SKOGSMO and A. ATRENS, *Acta Metallurgica et Materialia* **42** (1994) 1139.
32. A. ATRENS, G. DANNHAEUSER and G. BAERO, *J. Nuclear Mater.* **126** (1984) 91.
33. A. ATRENS, J. J. BELLINA, N. F. FIORE and R. J. COYLE, "*The Metals Science of Stainless Steels*," edited by W. E. Collings and H. W. King (TMS-AIME, 1978) 54.
34. J. G. WILLIAMS, C. R. KILLMORE, F. J. BARBARO, J. PIPER and FLETCHER, *Mater. Forum*, 1996, **20**, 13.
35. J. P. BENEDICT, R. ANDERSON, S. J. KLEPEIS and M. CHAKER, *Mat. Res. Soc. Symp. Proc.*, **199** (1990) 189.
36. M. X. ZHANG, "Crystallography of phase transformations in steels," PhD thesis, in University of Queensland, (1997) 135.
37. M. MILITZER, R. PANDI and E. B. HAWBOLT, *Metall. Trans.*, A, **27A** (1996) 1547.
38. R. F. MEHL and W. C. HAGEL, *Progr. Metal. Phys.* **6** (1956) 74.
39. A. K. SINHA, "Ferrous Physical Metallurgy" (Butterworths, 1989).
40. R. W. K. HONEYCOMBE and H. K. D. H. BHADESHIA, "Steels" (Edward Arnold, 1981).
41. M. X. ZHANG and P. M. KELLY, submitted to *Met. Trans.*

Received 1 June
and accepted 26 August 1998